N73 18826

CALIFORNIA INSTITUTE OF TECHNOLOGY

PASADENA, CALIFORNIA 91109

FINAL REPORT

on

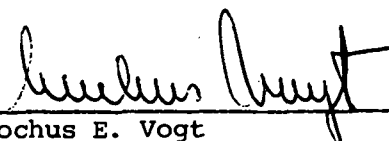STUDIES PERFORMED UNDER

NATIONAL AERONAUTICS AND SPACE ADMINISTRATION

GRANT NGR 05-002-225

1 JULY 1971 - 30 SEPTEMBER 1972

Rochus E. Vogt
Professor of Physics
Principal Investigator

TABLE OF CONTENTS

FINAL REPORT
NASA Grant NGR 05-002-225
California Institute of Technology
1 July 1971 — 30 September 1972

This report covers the studies performed by the Space Radiation Laboratory at the California Institute of Technology under NASA Grant NGR 05-002-225 in support of the mission definition phase of the Outer Planets Missions.

The activities may be divided into two major categories:

I. Participation in the study activities of the NASA-formed
Energetic Particles Team and of the Science Steering Group
for the OPM-project of the Caltech Jet Propulsion Laboratory (JPL) during mission definition.

II. Development and laboratory investigations of new particle
detectors and detector systems for the Outer Planets Missions

I.   Outer-Planets-Missions (OPM) Definition Studies.

For the OPM definition studies, NASA formed an Energetic Particles Team
(EPT), consisting of:

W. I. Axford, University of California – San Diego
S. M. Krimigis, Johns Hopkins Applied Physics Laboratory
F. B. McDonald, Goddard Space Flight Center
P. Meyer, University of Chicago
J. H. Trainor, Goddard Space Flight Center
J. A. Van Allen, University of Iowa
R. E. Vogt, California Institute of Technology

R. E. Vogt served as Team Leader, and S. M. Krimigis as Deputy Team Leader of the Energetic Particles Team .

The EPT's primary responsibility was the development of a scientific and technical rationale for the use of Energetic-Particle investigations in the exploration of the outer solar system and to assist the JPL project office in the design of the OPM spacecraft and mission objectives.

The Outer Planets Missions open up the outer solar system to intensive investigation. They provide a first opportunity to make quantitative comparative studies of the magnetospheres and radiation environments of the outer planets. They allow extensive exploration of the unknown outer regions of the interplanetary medium and of the heliospheric boundary, and they provide excellent opportunities to penetrate into the interstellar medium and to study cosmic rays, the most energetic component of the galaxy, beyond the influence of the solar wind.

The Energetic Particles Team met periodically during the OPM definition phase to develop science objectives, mission rationale, and to assist the JPL project office in the solution of technical problems. Parts of this work are reflected in the following reports generated by the EPT:

1.   "Energetic Particle Measurements on the Outer Planets Missions" (9 July 1971)

2.   "Energetic Particles Measurements on the Outer Planets Missions, Investigation Summary" (16 July 1971)

3.   "Energetic Particles Measurements on Minimum Science Payload OPGT Missions" (29 September 1971)

4.   "Energetic Particles Measurements on the Outer Planets Missions" (31 January 1972)

5.   "Energetic Particles Measurements on Outer-Solar-System Missions" (30 April 1972)

In addition, R. Vogt participated in a study, conducted by the Space Science Board of the NRC/National Academy of Sciences, on "Outer Planets Exploration," 8-14 August 1971, at Woods Hole, Mass. (see NRC/NAS report, "Outer Planets Exploration 1972-1985," National Academy of Sciences, Washington, D. C. 1971).

R. Vogt also gave presentations on science objectives of Energetic-Particles investigations on OP Missions to various NASA evaluation panels.

After completion of its objectives, the Energetic Particles Team dissolved in June 1972, and its individual members, in collaboration with other scientists, submitted separate proposals for participation in the Outer Planets Missions.

II.   Development and Investigation of Particle Detectors and Detector Systems.

The Caltech Space Radiation Laboratory (SRL) under direction of E. C. Stone and R. E. Vogt, considered the investigation and development of mission-unique solid-state-detector devices and cosmic-ray telescopes an important objective for the ultimate success of the Outer Planets Missions. The results of these investigations allow a realistic appraisal of the technical feasibility and the reliability of cosmic-ray and trapped-particle detector systems designed to accommodate the unique constraints and opportunities of the Outer Planets Missions.

In addition to the usual environmental conditions of space missions (e.g., vacuum, thermal environment, power restrictions, mechanical and acoustical strains, etc.) the Outer Planets Missions present other and new constraints in the performance of high-quality cosmic-ray observations. Among these are:

Extended mission lifetime - requiring extended reliability and stability of components.

Intense radiation environments, affecting the charge collection properties and survival rate of solid state devices.

Intense radiation background due to the Radioisotope Thermo-electric Generators (RTG's), causing both continuous real time interference and lattice defects.

A non-spinning spacecraft and considerable weight restrictions on the payload, demanding design of minimum-weight telescopes.

The Caltech Space Radiation Laboratory (and colleagues from the Goddard Space Flight Center and the University of New Hampshire, who have formed an investigator team for the OP missions) considers the use of all-solid-state particle telescopes of prime importance for the accomplishment of the funda-mental scientific objectives. The choice of all-solid-state telescopes, with novel solid-state anticoincidence guards instead of the usual scintillator-photomultiplier guard counters, is dictated by considerations of stability, sensitivity, reliability, and weight and high-voltage requirements. In addition, the crucially important measurements of potentially small anisotropies of cosmic-ray fluxes from a 3-axis stabilized spacecraft require rotation devices for the particle telescopes, both for scanning and intercalibration. Such rotation devices[1] can be built economically and reliably (within realistic S/C con-straints) only for small, light-weight telescopes, i.e. of all-solid-state con-struction.

In the pursuit of these investigations, the Caltech SRL concentrated upon triple groove silicon devices (center active element + ring active element + active guard electrode), shown in Figures 1 and 2, while the GSFC investigated double-groove devices[2] (outer active element + ring active ele-ment, without guard). These two independent approaches were considered essen-tial in view of the time constraints of the program. The double-groove devices are clearly simpler and therefore preferable. However, it was not certain whether they would have the necessary energy resolution, stability and ease of manufacturability, whereas, the more complex triple-groove devices appeared more promising on purely theoretical grounds. In the final analysis, both types of devices proved to be satisfactory; however, only after experience with triple-groove devices provided essential technical feedback for double-groove devices to the design engineers of the manufacturer.

1) Triple-groove LID Solid-State Detectors

The solid-state detectors were developed and manufactured by the Nuclear Physics Division of KEVEX Corporation, Burlingame, California under close supervision and technical consultation of Caltech and GSFC personnel.

The configuration of the LID detectors which were tested by Cal-tech's SRL is shown in Figure 2. This configuration can be referred to as a triple-groove detector, since the n-type contact is cut by 3 concentric grooves so that the area of the single wafer of silicon is divided into 3 electrically separate areas.

---

[1] A working rotation device has been built and fully tested at GSFC and is incorporated in our MJS proposal.

[2] The results of the GSFC investigations appear in separate GSFC reports. GSFC has also undertaken a full radiation testing program of these detectors for the effects of intense particle fluxes and fluences.

The central circular area A of the detector is the primary detector of the three. The adjacent ring B is designed to serve as an anti-coincidence detector, so that particles which penetrate area A and exit through area B can be rejected without further analysis. The second ring (C) is a guard ring which provides a separate path for the larger leakage currents often associated with the edges of the silicon wafer. The particle detection characteristics of the guard ring C were also investigated.

The triple groove detectors were subjected to the standard detector tests which have been developed in the Caltech Space Radiation Laboratory in support of solid-state-detector telescopes which have been launched on OGO-2, OGO-4, OGO-6, and IMP-H/J. Eight examples of these tests are listed in Table I and summarized below.

TABLE I: Tests of Solid-State Detectors

A. Electrical characteristics

  1. Leakage current as a function of bias voltage.

  2. Leakage current as a function of temperature.

B. Charge Collection Efficiency

C. Charged Particle Response

  1. Energy resolution for alpha particles.

  2. Anticoincidence efficiency for penetrating particles.

  3. Alpha-particle size scan.

  4. Penetrating-electron size scan.

D. Surface Effects

A. Electrical Characteristics

1. Leakage current as a function of bias voltage

The reverse bias current-voltage characteristics of each detector diode is carefully measured in order to determine the stable operating range. Figure 3 shows the results for each of three sensitive areas for two different detectors. The current-voltage characteristic of the central area and the anticoincidence ring are similar in both cases, while the guard ring exhibits a much higher leakage current. In all cases, however, stable operation was possible with up to at least 500 V applied bias.

2. Leakage current as a function of temperature.

On the basis of the room temperature test, a bias voltage
of 491 V was applied to the three sensitive areas of each
detector and the leakage current was measured as a function of
temperature. Results for two of the detectors are shown in
Figure 4. The devices functioned properly over the temperature
range up to 45° C.

B. Charge Collection Efficiency

The operating bias voltage of a detector must be high enough to
ensure almost complete charge collection efficiency, so that the
measured signal is directly relatable to the energy loss of the in-
cident particle. To determine the minimum operating voltage, the
detectors were exposed to a beam of 8.785-MeV alpha particles incident
on the p-contact (see Fig. 2). The charge signal was measured as a
function of the applied bias voltage. The results for one detector
are shown in Figure 5. An operating bias as low as 250 V would satisfy
the requirement of full charge collection for alpha particles.

C. Charged Particle Response

1. Energy resolution for alpha particles

Each detector was exposed to 8.785-MeV alpha particles in
order to determine its resolution characteristics. A fixed
bias voltage of 491 V was applied to all 3 sensitive areas of
each detector, and the alpha resolution was measured for each
of the areas. Results for detector #1590 are shown in Figure 6.
All three areas exhibit acceptable alpha-particle-resolution,
although the guard ring has somewhat lower resolution than the
center and anticoincidence ring. Thus in many instances the
guard ring could serve as an anticoincidence and the separate
anticoincidence ring could be eliminated.

2. Anticoincidence efficiency for penetrating particles

Since the triple groove detectors are designed to measure
not only stopping particles but also penetrating particles, each
detector was tested with a beam of 1.8 MeV electrons from a
β-spectrometer. The results of one penetrating-particle test of
particular interest are shown in Figure 7, where two measured
energy-loss distributions for 1.8 MeV β-particles are compared.
In both cases, the electrons were incident near one edge of the
center area, so that edge effects such as the scattering of some
electrons out of the collection region of the center area produce
some energy-losses which are too small. The distribution with
circles clearly shows the edge effect by the large number of counts
below 600 keV. The distribution with solid dots, however, is

much freer of edge effects. This second distribution was
obtained by rejecting for analysis all events which produced
a measurable signal in the adjacent anticoincidence ring. This
marked reduction in edge effects is an especially important
feature of the integral anticoincidence ring.

3.   Alpha-particle size scans

The size and location of each of the 3 sensitive areas on
each detector were determined by measuring the alpha-particle
counting rate due to a source which was scanned along a detector
diameter. One such alpha scan is shown in Figure 8. For
comparison, a cross-section diagram of the detector shows the
physical location of the 3 concentric grooves which define the
3 sensitive areas.

4.   Penetrating electron size scans

The size and location of each sensitive region was also
determined by scanning along a detector diameter with a 1.8
MeV electron beam. The measured counting rate as a function
of beam position is shown for one detector in Figure 9. Because
the electrons scatter significantly on penetrating the detector,
the edges of each region are diffuse and the response curves of
adjacent regions overlap. This overlap is greatly reduced by
placing adjacent areas in anticoincidence, so that only particles
remaining within a single area are counted or analyzed.

D.   Surface Effects

The n-type contact is a relatively thick layer of low resistivity
material from which no signal is collected. The thickness of this
dead layer was measured with alpha particles and was found to be
between 48 ± 1 and 52 ± 1 μm of silicon for the various detectors. The
p-type contact has a much thinner dead layer which was measured to
be 0.3 ± 0.2 μm of silicon equivalent. These dead layers were within
specification.

2)   Development of an Electron Telescope (TET)

During the OPM definition studies it became clear that the spacecraft
and payload constraints of the Outer Planets Missions would make it un-
likely that a full and ideal complement of cosmic-ray detectors could be
accommodated. When requested to investigate and discuss "Minimum Science
Payloads," the Energetic-Particles Team consistently emphasized the priority
of investigations of the charge, mass, and energy spectra of cosmic-ray
nuclei below energies of about 500 MeV/nucleon. It was impossible,
realistically, to accommodate a standard electron telescope (which weighs
typically about 10 pounds). On the other hand, the EPT, the SSG and various
other scientific advisory groups continued to emphasize the extreme
scientific importance of electron studies, particularly in the low energy

region, where no information on galactic phenomena can be deduced from observations near Earth.

A. Scientific Rationale

The measurement of the galactic intensity of electrons, specifically below $\approx$ 100 MeV, will have a profound effect on our understanding of the role of these electrons in producing the diffuse x- and γ-ray background in the galactic disk, in understanding the dynamics of the galactic disk-halo magnetic-field relationship, as well as understanding the method of escape of these electrons from known source regions such as the Crab Nebula.

Above a few hundred MeV, the electron spectrum near the Earth is reasonably well known, and, although less well understood, the broad features of the solar modulation have also been extensively measured and can be adequately determined at the orbit of Earth. The understanding of the modulation at rigidities >100 MV, to be gained from the study of nuclei on the MJS missions, makes it possible to determine the galactic spectrum of electrons >100 MeV outside of the solar cavity. Furthermore, using estimates of galactic radio emissivity obtained from measurements of non-thermal radio emission, under the assumption that this radio emission is caused by synchrotron radiation by energetic electrons in galactic magnetic fields, it is also possible to deduce the interstellar electron spectrum. A comparison of the galactic electron spectra obtained from these two approaches may be used to examine the spatial distribution of electrons and magnetic fields in the galaxy.

It should be noted that the radio measurements extend down to only ~ 1 MHz, which corresponds to a few hundred MeV electron energy in the galactic magnetic fields. Below a few hundred MeV, we can only speculate on the interstellar electron spectrum. For example, the low-energy galactic radio spectrum is observed to turn over and decrease below 1 MHz. It is usually assumed that this is due to free-free absorption by interstellar hydrogen. But it is possible that the electron spectrum itself turns over as well at the equivalent energies. Obviously, the correct interpretation of this feature is of fundamental importance in understanding the conditions in the interstellar medium (e.g., the presence of cold gas clouds and the temperature of the intercloud medium) and for the understanding of the origin of these electrons and their importance in galactic dynamics.

If one extends the interstellar electron spectrum above 300 MeV, as deduced from radio background measurements, down to below 20 MeV, then this spectrum exceeds that observed at Earth by a factor of >1000! Yet the spectrum observed at Earth is roughly consistent with an interstellar knock-on origin for these electrons without invoking an additional, perhaps primary, source. Is this difference due to extremely large solar modulation effects or is the interstellar spectrum at low energies really not much different than at Earth? Some of the rich possibilities for the behavior of the low-energy electron spectrum in interstellar space are illustrated in Figure 10. The resolution of this problem requires measurements of electrons specifically below 100 MeV.

B. Experimental Approach

   The Caltech Space Radiation Laboratory therefore concentrated
on the possibility of developing a small, lightweight electron
telescope (design goal: ~ 1 lb.) which could be added to the MJS
payload and cover the crucial energy range for electrons between
~ 5 - 150 MeV, which range cannot be covered by the nuclei-detector
systems of energetic-particle experiments.

   We have been able to design, test, and calibrate a relatively
simple, small, and light-weight electron energy spectrometer in the
5-110 MeV energy range. The use of novel integral detector-guarding
devices (see Sec. B-1) allows an all-solid-state detector design with
adequate energy resolution and background rejection so that meaning-
ful spectra can be measured even at the relatively low electron in-
tensities near Earth. The response of the electron telescope, includ-
ing the effects of background, have been verified by accelerator cali-
brations (with support from the GSFC group) of a prototype model and
by Monte-Carlo calculations.

   Figure 11 represents a schematic cross-section of the principal
features of a prototype electron-telescope developed by the SRL for
the MJS missions. It consists of an array of solid-state detectors
and absorbers in a cylindrical geometry, surrounded by a grid of
solid-state guard detectors. In the prototype model shown, electrons
and their energies are identified by a double-dE/dx measurement in
detectors D_1 and D_2 and by a simultaneous measurement of their range,
as determined by the penetration of detectors D_3 through D_7. The
use of range spectroscopy, while providing satisfactory energy
resolution and background rejection (see below), has the additional
virtue of being insensitive to electronic gain drifts which may arise
in MJS-type long-term missions.

   The prototypes calibrated on accelerators over an energy range
of ~1 MeV to ~1 GeV did not contain the solid-state guardring devices
(unavailable within the restricted budget of this study) but rather
conventional solid-state detectors available in our laboratories.
However, the guard devices had no intrinsic bearing on the range-energy
calibrations performed. They mainly affected the Monte-Carlo calcula-
tions for detection efficiency and background rejection, where they
were fully considered. The energy-response data derived from acceler-
ator calibrations showed an equivalent energy resolution comparable
in quality to those of conventional (and much heavier) total-energy-
absorption devices. The response curves form the basis of a convers-
ion matrix which is used to unfold energy spectra from range distribu-
tions, as illustrated in Figure 13 and Table II. The three energy
spectra used for illustration purposes represent realistic estimates
for the MJS missions. The interstellar electron spectrum shown is
based upon the galactic non-thermal radio spectrum for energies above
several hundred MeV and represents a power-law extrapolation at lower
energies. The spectra shown for 5 AU and 1 AU have been derived
from the interstellar spectrum by use of numerical solutions of the
cosmic-ray transport equation using accepted values for the solar wind
velocity and the cosmic-ray diffusion coefficients. In addition, the
calculated electron spectrum at 1 AU agrees with observational results.
The 1 AU spectrum shown may be considered typical for the expected
electron fluxes at the beginning of the MJS '77 missions.

TABLE II: Telescope Range Distributions and
Maximum Background Levels for Three
Typical Cosmic-Ray Electron Spectra
Shown in Figure 13.

Range (D$_i$'s triggered)	Geometry Factor (cm^2-sr)	Counts/Month			
		1 AU	5 AU	Interstellar	Max Background
D$_1$D$_2$D$_3$	1.8	1.8×10^3	3.4×10^4	1.6×10^6	3.9×10^2
D$_1$...D$_4$	1.4	1.6×10^3	1.6×10^4	5.2×10^5	5.2×10^2
D$_1$...D$_5$	1.0	1.4×10^3	8.6×10^3	1.7×10^5	5.2×10^2
D$_1$...D$_6$	0.8	1.4×10^3	6.0×10^3	7.3×10^4	5.2×10^2
D$_1$...D$_7$	0.6	1.4×10^3	4.9×10^3	4.2×10^4	7.8×10^2

As an example, we show in Table II the expected range distributions (determined from the calibrated detector response) for the three typical electron energy spectra shown in Figure 13. The application of a simple unfolding technique to these data results in the very satisfactory reproduction of the input spectra shown by the data points in Figure 8. The dashed areas in Figure 13 indicate conservative estimates of maximum background levels during the mission which are caused by the spacecraft RTG's (below ~2.5 MeV) or by interacting high-energy protons in the detector stack. The RTG background levels are obtained from direct calibrations of the GSFC/UNH Pioneer 10 telescope. The basic D$_1$D$_2$D$_3$ coincidence requirement, which includes the absorber A$_1$, makes the electron telescope insensitive to RTG-background. The proton induced background (above ~2.5 MeV) has been calculated by Monte-Carlo techniques for the maximum flux levels of primary cosmic rays during the MJS missions. The Monte-Carlo programs and the nuclear cross sections used in the calculations have been successfully applied by the Caltech laboratory to other cosmic-ray telescopes with extensive verifications on particle accelerators and in nature. Definitive electron energy spectra can be measured for all phases of the MJS missions without significant background interference.

FIGURE CAPTIONS

Figure 1   Photograph of a "triple-groove" LID detector.

Figure 2   Schematic diagram of the triple-groove detector.

Figure 3   Detector leakage currents versus applied bias at room
               temperature.

Figure 4   Detector leakage currents versus temperature at 491 V
               applied bias.

Figure 5   Measured alpha-particle energy versus applied bias voltage.
               The incident alpha-particle energy was 8.785-MeV and was
               incident on the p-contact of the detector (see Figure 2).

Figure 6   Energy resolution for 8.785-MeV alpha particles incident
               on the p-contact for each of the 3 sensitive areas of
               detector #1590.

Figure 7   Energy-loss spectra of penetrating electrons incident on
               one edge of the central sensitive area. The spectrum with
               open circles was accumulated without regard for any response
               in the anticoincidence ring. The spectrum with closed
               circles illustrates the effect of analyzing only those events
               which are not accompanied by a signal from the anticoincidence
               ring.

Figure 8   Alpha-particle counting rate as a function of source position
               on detector #1601. The counting rate is measured as a function
               of position of the source as the source is moved along a
               detector diameter. The response in each of the 3 sensitive
               areas is indicated, as are the physical locations of the 3
               concentric grooves.

Figure 9   Penetrating-electron counting rate as a function of the position
               of the incident beam. Due to the scattering of electrons, the
               edges of the 3 sensitive areas are more diffuse for electrons than
               for alpha particles. For comparison, the physical location of
               the 3 sensitive areas is also indicated.

Figure 10   Electron spectra observed at Earth and limits on possible spectra
               for the MJS missions.

Figure 11   Schematic cross section of a SRL prototype MJS electron telescope.

Figure 12   Typical electron spectra (solid lines) for heliocentric radii of
               1 AU, 5 AU, and the interstellar medium. Data points show the
               response and resolving power of the prototype electron telescope
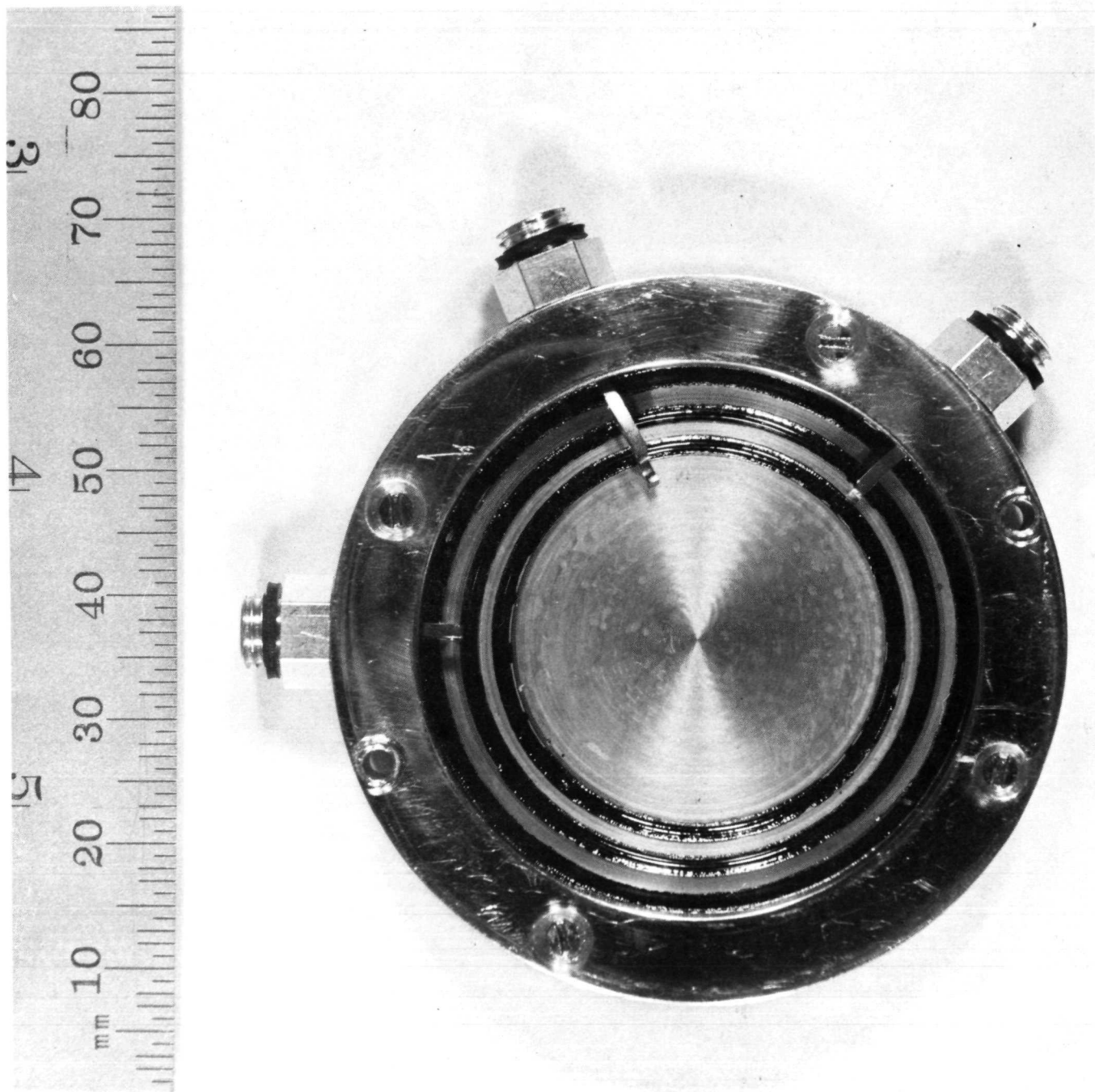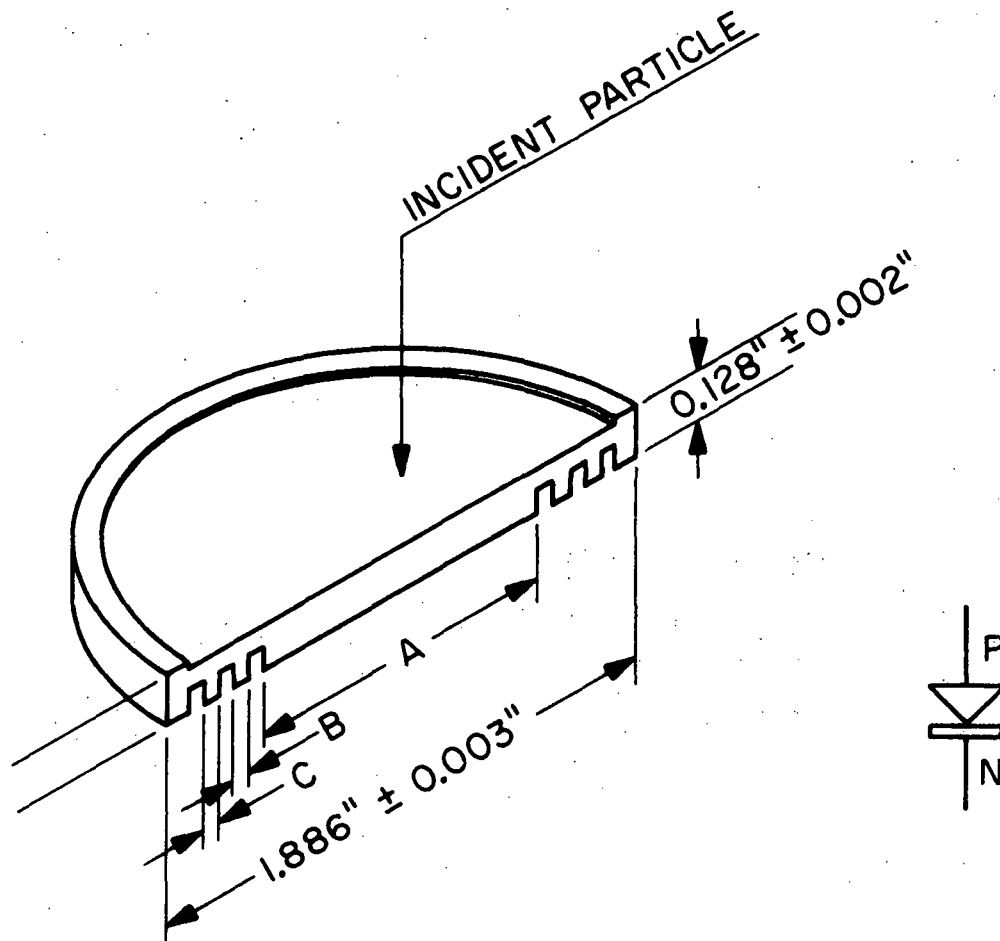   to these spectra.

Fig. 1

INCIDENT PARTICLE

0.128" ± 0.002"

A

B

C

1.886" ± 0.003"

P

N

		AREA IN MM^2
A	CENTER DETECTOR	850 MM^2
B	ANTI COINC.	200 MM^2
C	GUARD RING	200 MM^2

Fig. 2
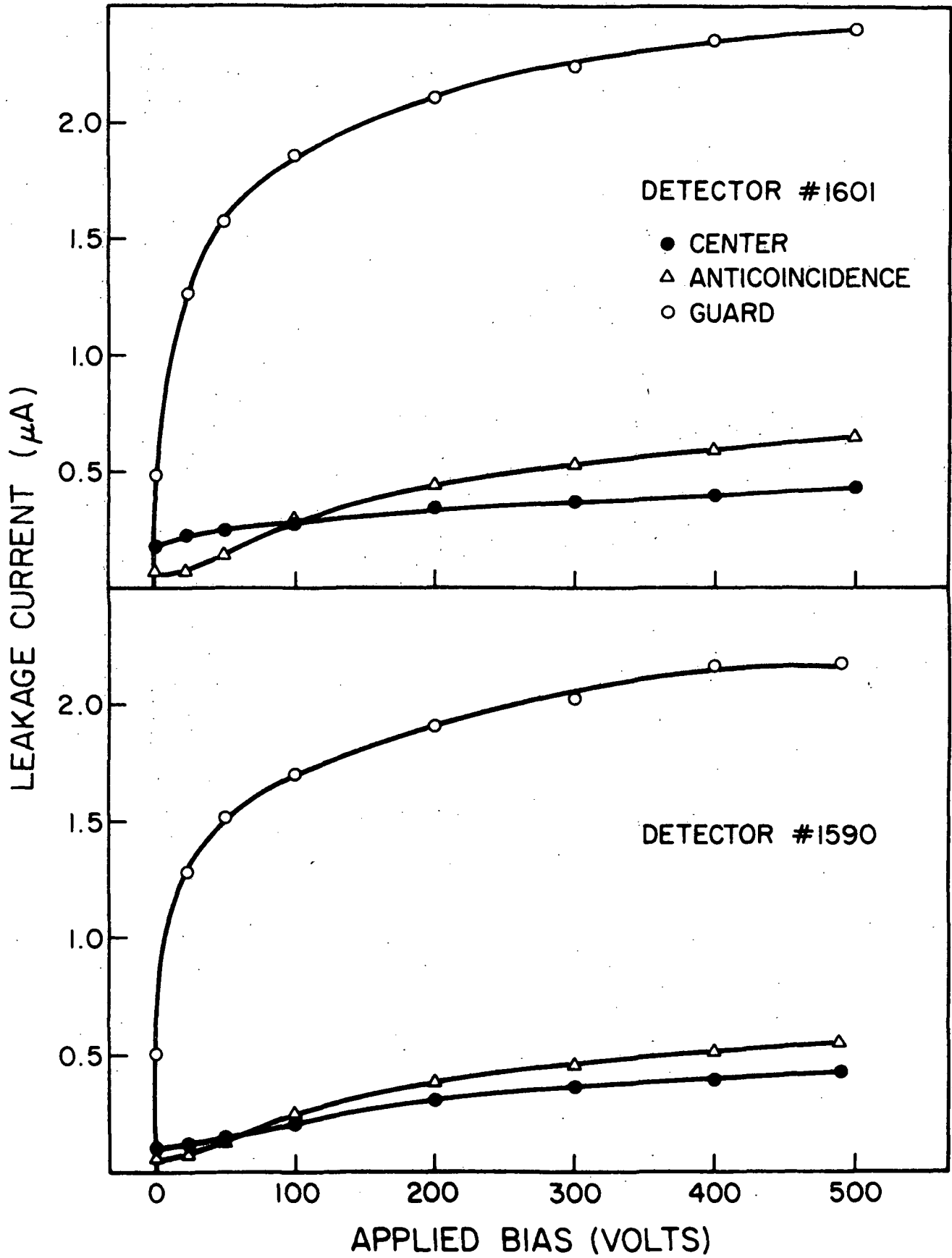
Fig. 3
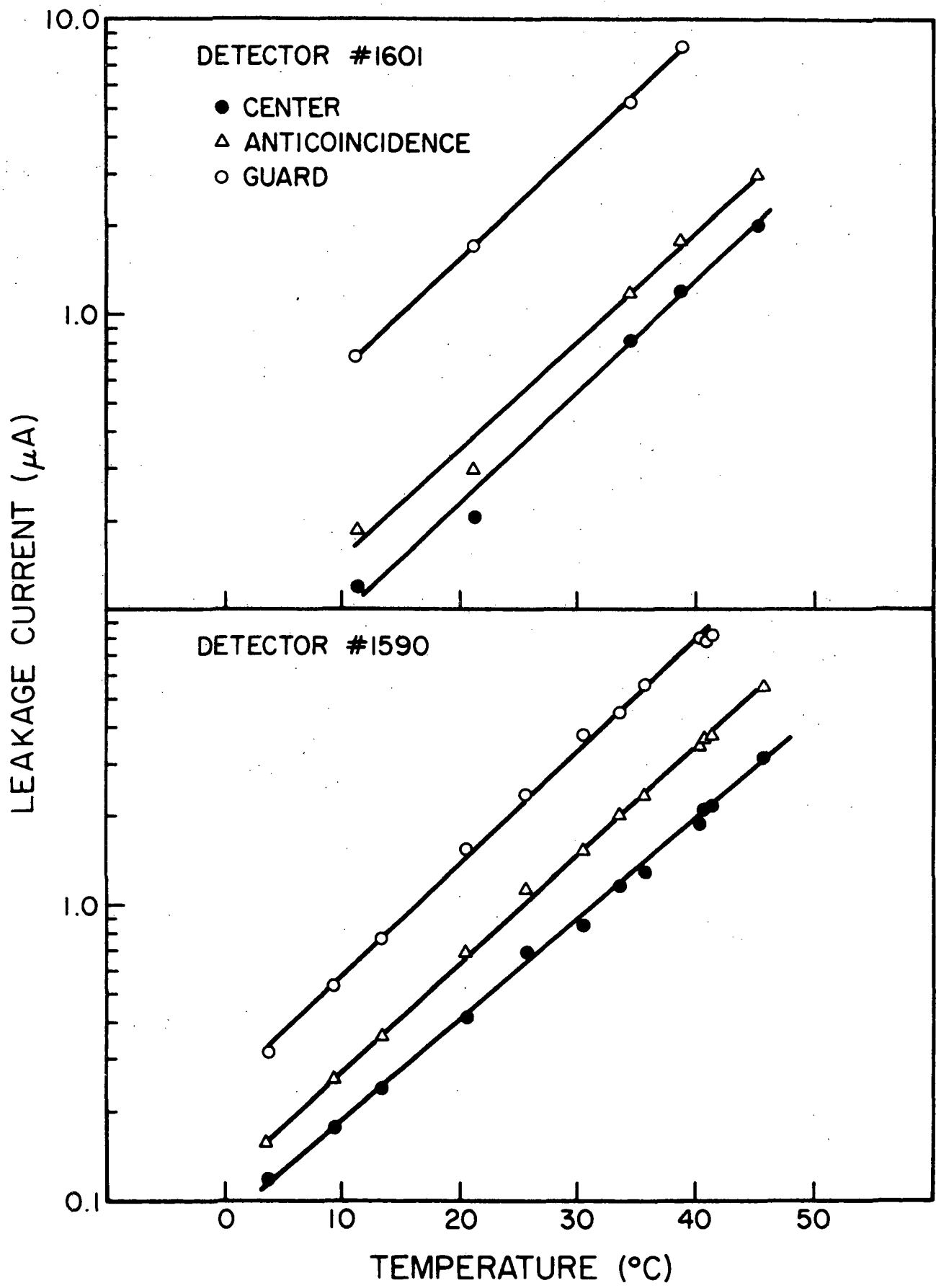
Fig. 4
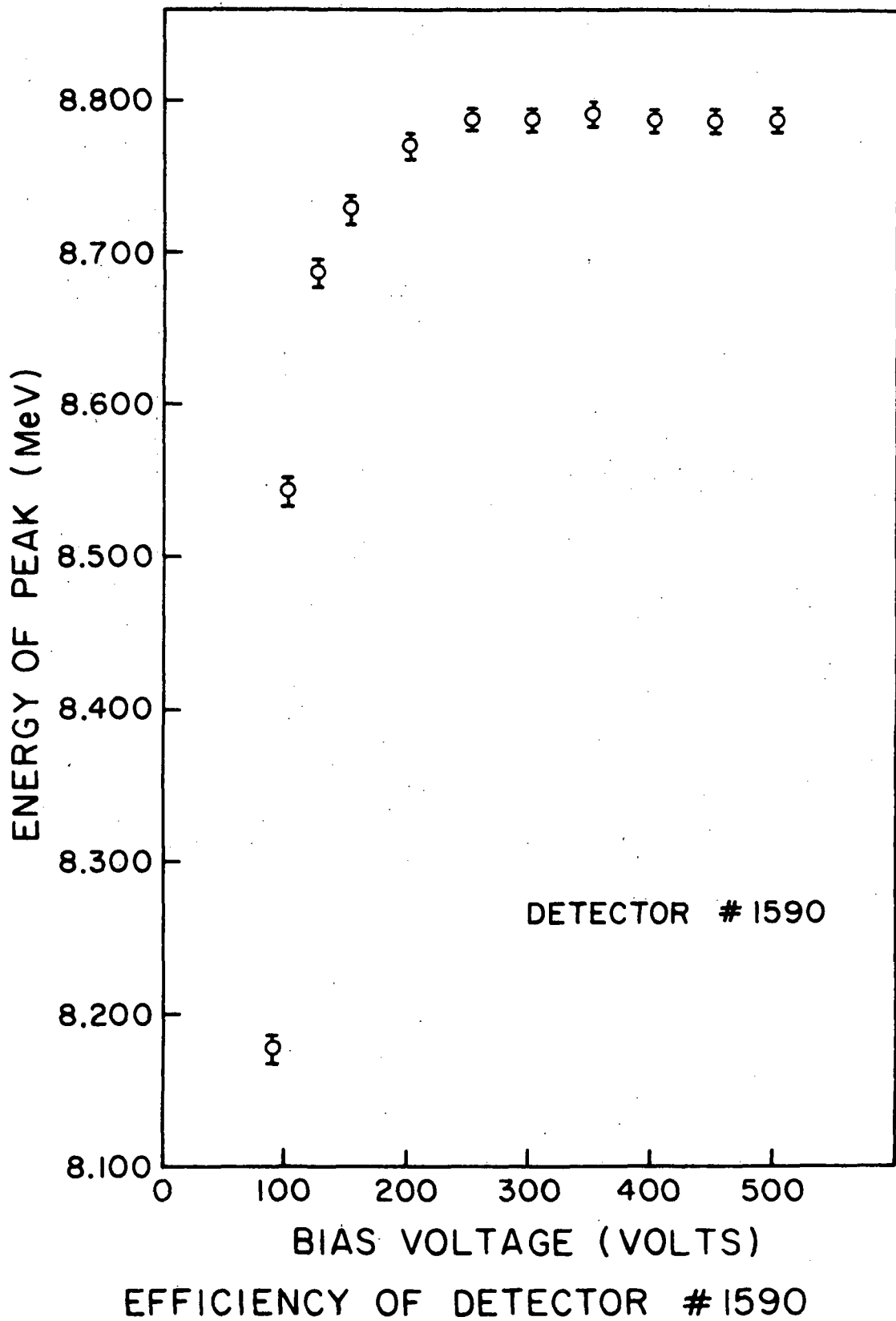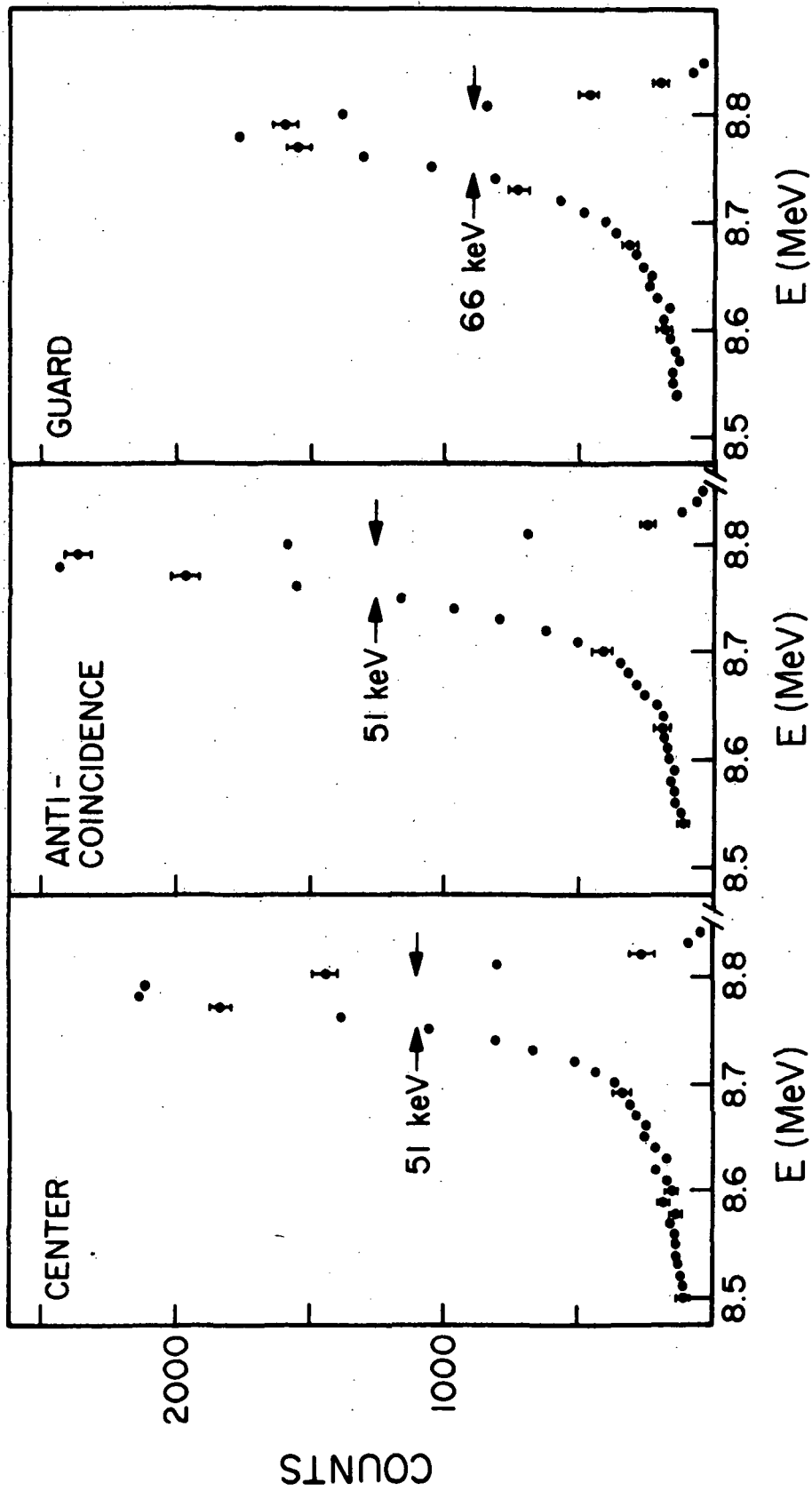
EFFICIENCY OF DETECTOR #1590

Fig. 5

Fig. 6

Fig. 7

CROSS-SECTION ALONG A DIAMETER OF A
TYPICAL DETECTOR BY OPTICAL SCAN

● CENTER
○ ANTI-
  COINCIDENCE
△ GUARD

CENTER

CM

-2.0   -1.0   0.0   1.0   2.0   3.0

COUNTS (ARBITRARY)

Fig. 8

Fig. 9

Fig. 10

D₁

D₂ — A₁ = 0.5 mm
D₃ — A₂ = 1.0 mm
D₄ — A₃ = 1.5 mm
D₅ — A₄ = 2.0 mm
D₆ — A₅ = 2.5 mm
D₇ — A₆ = 3.0 mm
D₈

Solid-state guard
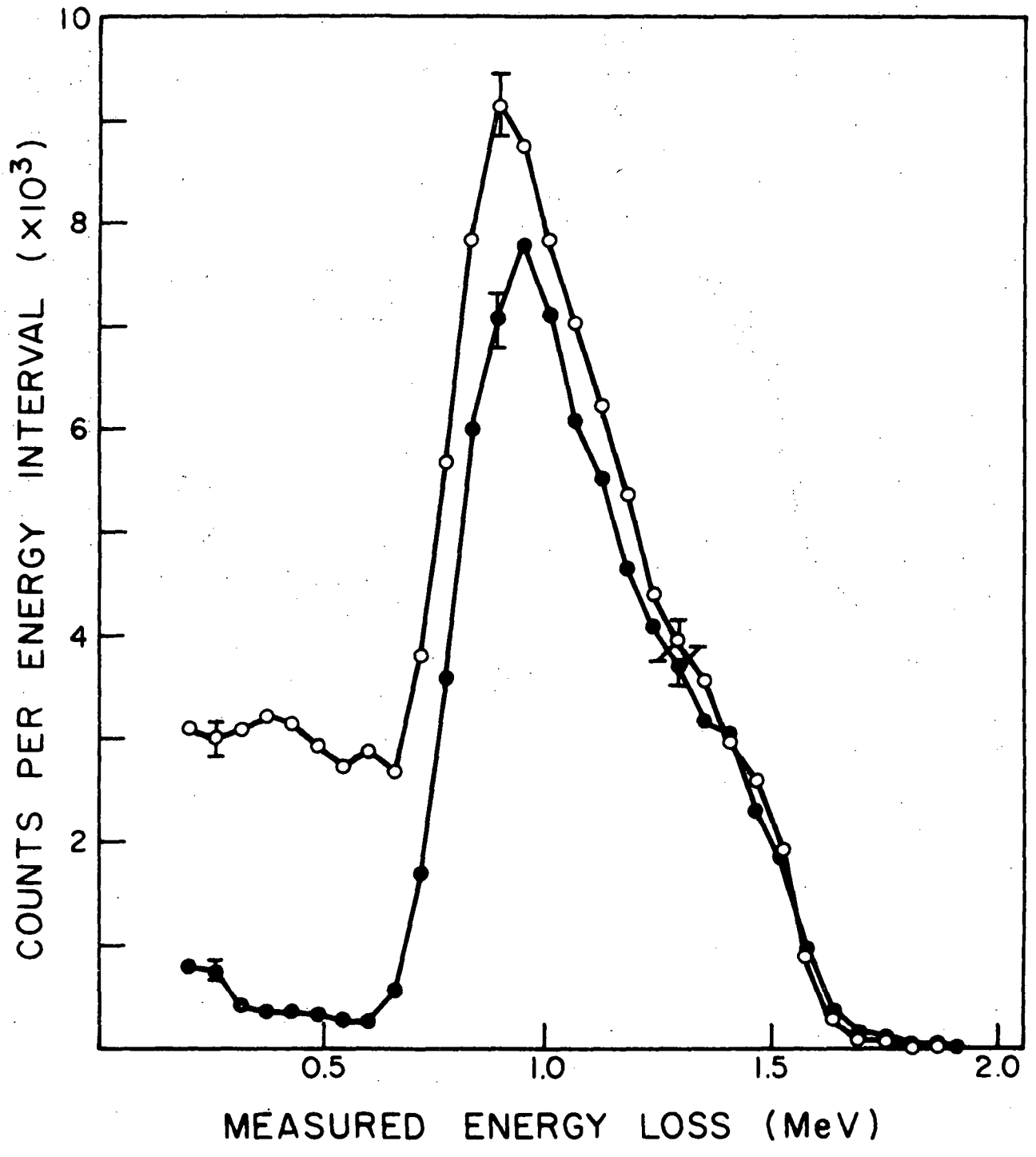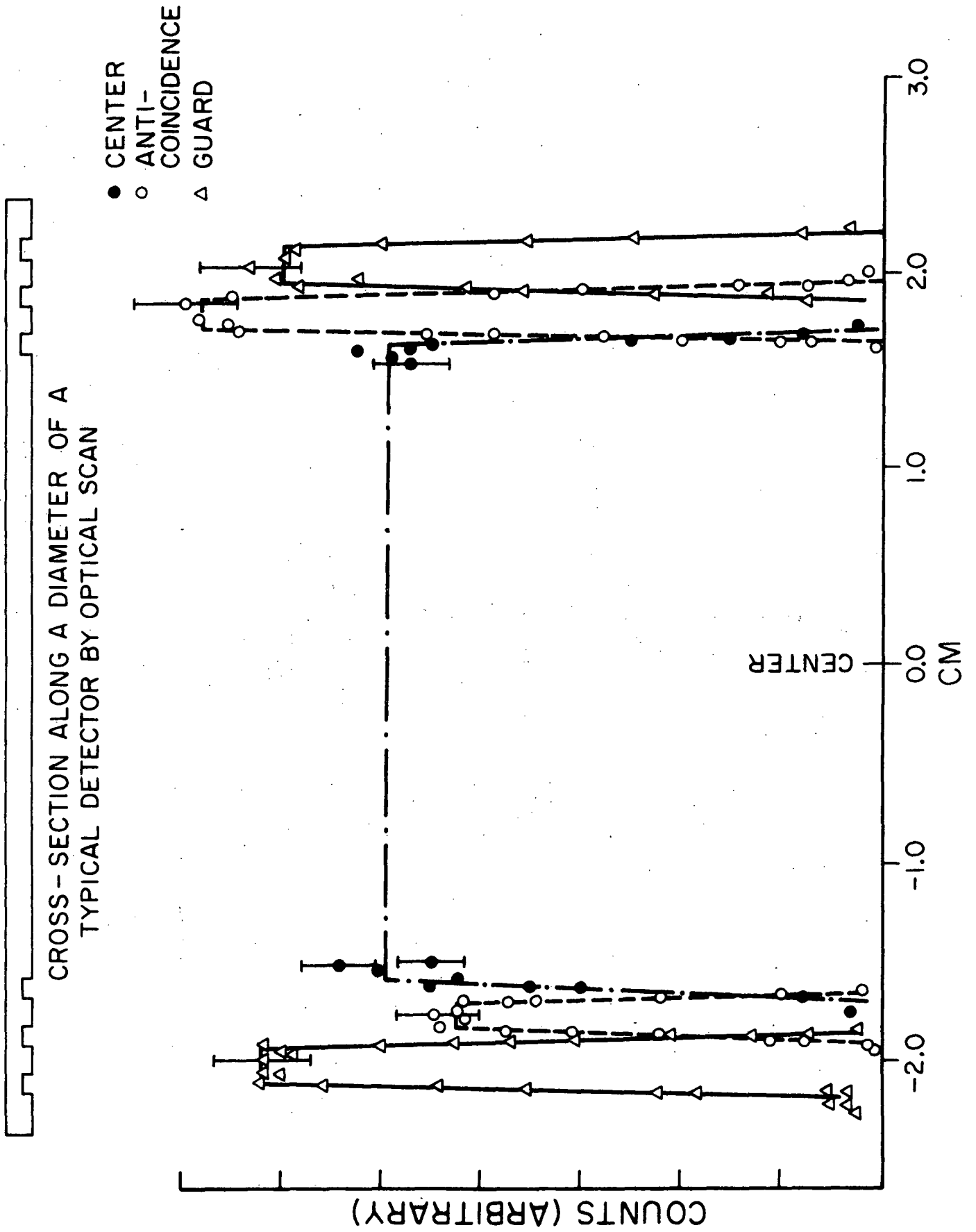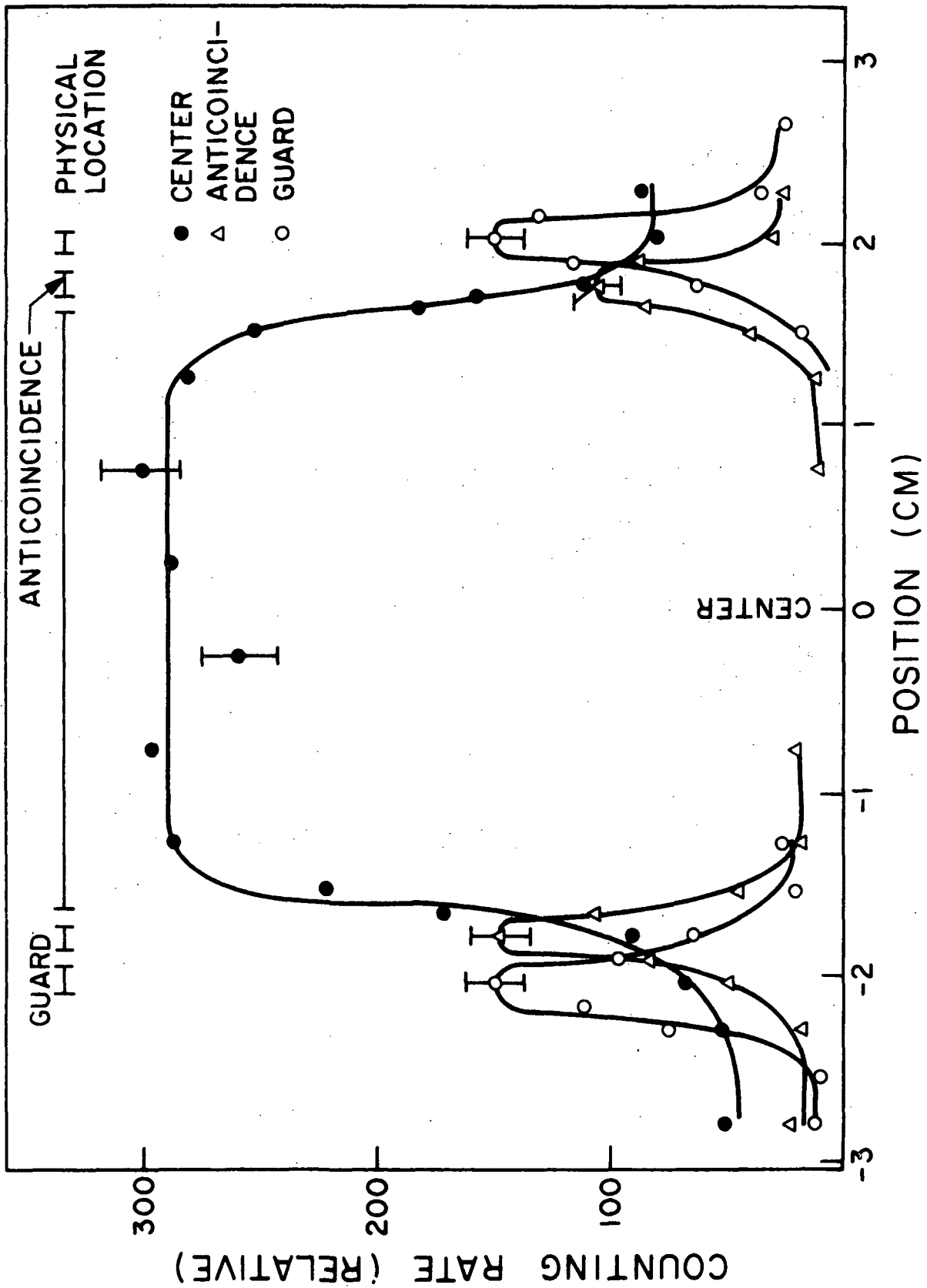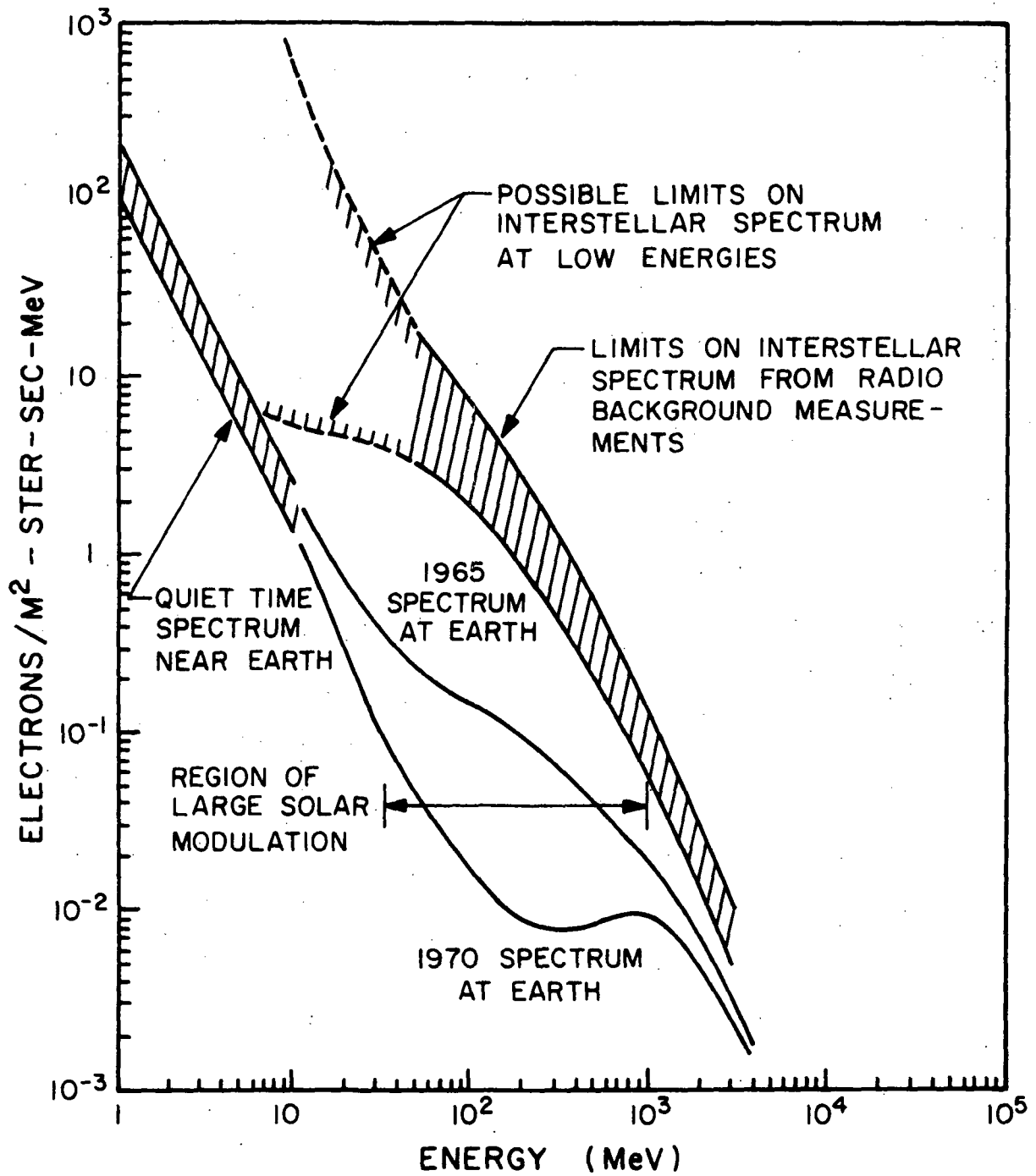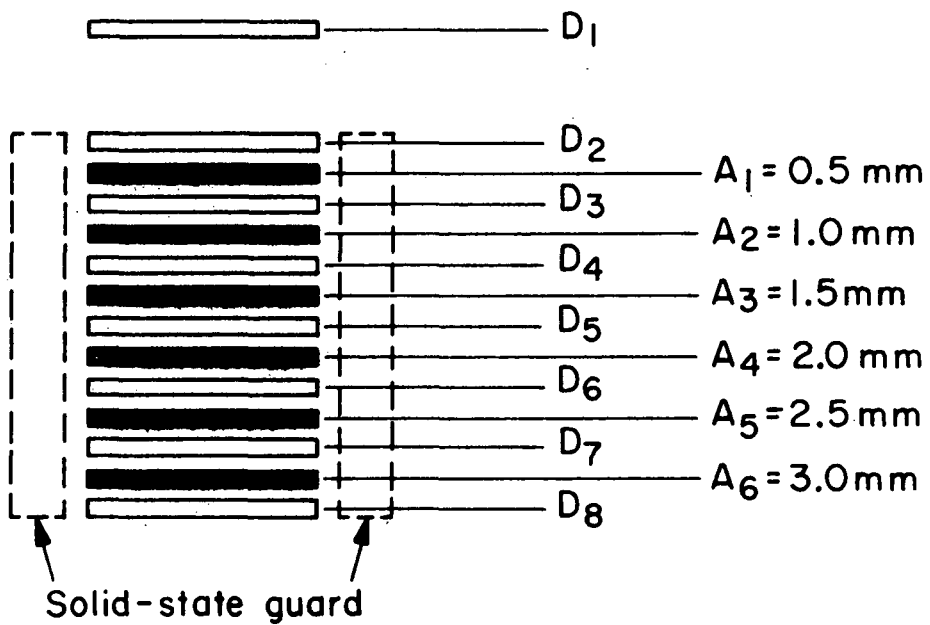
D_i = 2.5 mm LID detectors

A_i = tungsten absorbers

Fig. 11

Fig. 12